Synchronization phenomena observed in glacial-interglacial cycles simulated in an Earth system model of intermediate complexity

Takahito Mitsui[1,2], Matteo Willeit[2], and Niklas Boers[1,2,3]

[1]Technical University of Munich, Germany; School of Engineering & Design, Earth System Modelling
[2]Potsdam Institute for Climate Impact Research (PIK), Member of the Leibniz Association, P.O. Box 6012 03, D-14412 Potsdam Germany
[3]Department of Mathematics and Global Systems Institute, University of Exeter, UK

Correspondence: Takahito Mitsui (takahito321@gmail.com)

Abstract. The glacial-interglacial cycles of the Quaternary exhibit 41-kyr periodicity before the Mid-Pleistocene Transition (MPT) around 1.2–0.8 Myr ago and ∼100-kyr periodicity after that. From the viewpoint of dynamical systems, proposed mechanisms generating these periodicities are broadly divided into two types: (i) nonlinear forced responses of a mono- or multi-stable climate system to the astronomical forcing, or (ii) synchronization of internal self-sustained oscillations to the

5 astronomical forcing. In this study, we investigate the dynamics of glacial cycles simulated by the Earth system model of intermediate complexity CLIMBER-2 with a fully interactive carbon cycle, which reproduces the MPT under gradual changes in volcanic CO_2 degassing and regolith cover. We report that, in this model, the dominant frequency of glacial cycles is set in line with the principle of synchronization. It is found that the model exhibits self-sustained oscillations in the absence of astronomical forcing. Before the MPT, glacial cycles synchronize to the 41-kyr obliquity cycles because the self-sustained

10 oscillations have periodicity relatively close to 41 kyr. After the MPT the time scale of internal oscillations becomes too long to follow every 41-kyr obliquity cycle, and the oscillations synchronize to the 100-kyr eccentricity cycles that modulate the amplitude of climatic precession. The latter synchronization occurs with the help of the 41-kyr obliquity forcing through a mechanism that we term vibration-enhanced synchronization. While we interpret the dominant periodicities of glacial cycles as the result of synchronization of internal self-sustained oscillations with the astronomical forcing, the Quaternary glacial

15 cycles show facets of both synchronization and forced response.

1 Introduction

Glacial-interglacial cycles are pronounced climatic oscillations accompanied by massive changes in the global ice volume (Rohling et al., 2014; Spratt and Lisiecki, 2016), greenhouse gas concentrations (Bereiter et al., 2015; Lüthi et al., 2008; Petit et al., 1999), and temperatures (Jouzel et al., 2007; Snyder, 2016). Changes in global ice volume are recorded, e.g., in the

20 oxygen isotope ratio $\delta^{18}O$ of benthic foraminifera in marine sediments (Lisiecki and Raymo, 2005) (Fig. 1d, black), where higher $\delta^{18}O$ values indicate larger ice volumes and cooler deep-ocean temperatures. The glacial cycles have relatively small-amplitude oscillations with dominant 41-kyr periodicity until ∼1.2–0.8 million years before present (Myr BP), while during the more recent part of the Pleistocene, they are characterized by larger amplitudes and a dominant periodicity of ∼100-kyr
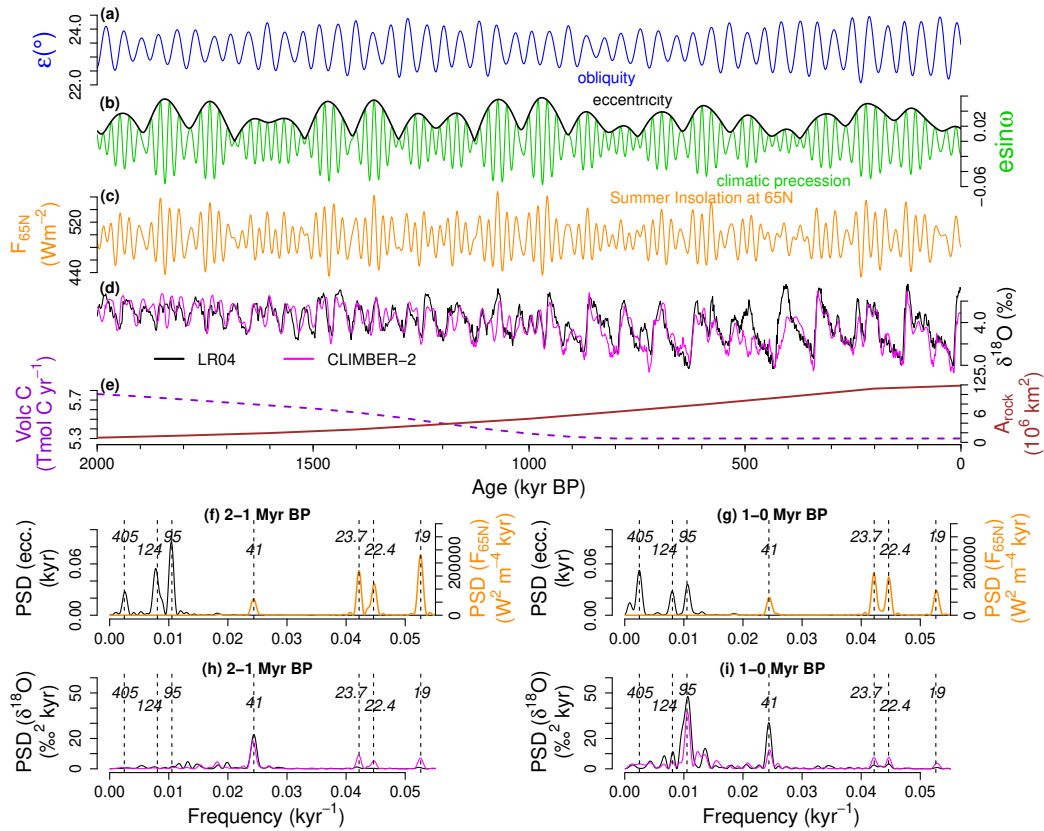
Figure 1. Time series and power spectral densities (PSD) of the astronomical forcing (Laskar et al., 2004) and glacial cycles over the last 1 Myr. (a) Obliquity (blue). (b) Climatic precession (green) and eccentricity (black). (c) Boreal summer solstice insolation at $65°$N. (d) LR04 δ^{18}O stack (Lisiecki and Raymo, 2005) (black) representing glacial-interglacial cycles during the last 2 Myr and corresponding CLIMBER-2 δ^{18}O simulation by Willeit et al. (2019) (magenta) under the optimal background condition scenario shown in (e). Note that the vertical axis is reversed so that larger δ^{18}O values, corresponding to colder conditions, are lower. (e) Optimal scenario (Willeit et al., 2019) for the volcanic CO_2 (Volc C) outgassing rate (violet, dashed) and the area of exposed crystalline bedrock, A_{rock} (red, solid). (f) PSD of the eccentricity (black) and the PSD of the summer solstice insolation F_{65N} (orange) over the interval from 2 Myr to 1 Myr before present (BP). (g) same as (f) but over the interval from 1 Myr to present. (h) PSD of the LR04 δ^{18}O record (black) and PSD of the optimal CLIMBER-2 simulation (magenta) over the 2 Myr-to–1 Myr interval. (i) same as (h) but over the 1 Myr-to-present interval. The dashed vertical lines in (f–i) indicate major astronomical periodicities (Laskar et al., 2004).

(black in Figs 1h and 1i). This transition is called the Mid-Pleistocene Transition (MPT), and its mechanisms and timing are
25   still debated (Berends et al., 2021; Clark et al., 2021; Ford and Chalk, 2020; Legrain et al., 2023).

There is general agreement that the glacial cycles are in some way paced by changes in the incoming solar radiation (i.e., insolation) caused by long-term variations of astronomical parameters (Hays et al., 1976; Huybers, 2011; Cheng et al., 2016; Tzedakis et al., 2017; Liautaud et al., 2020; Barker et al., 2022); (i) the obliquity ε (Fig. 1a) describes the Earth's axial

tilt and has a dominant periodicity around 41 kyr (Laskar et al., 2004), (ii) the eccentricity e of the orbit (Fig. 1b, black)

30 has dominant periodicities at 95, 124 and 405 kyr (Laskar et al., 2004), and (iii) the climatic precession $e \sin \omega$ (Fig. 1b, green), with dominant periodicities at 23.7, 22.4 and 19 (18.95) kyr (Laskar et al., 2004), varies with the longitude of the perihelion relative to the moving spring equinox ω, and its amplitude is modulated by the eccentricity, as shown in Fig. 1b. The dominant frequencies of climatic precession are mechanically related to those of the eccentricity: $1/19 - 1/23.7 \simeq 1/95 \text{ kyr}^{-1}$, $1/19 - 1/22.4 \simeq 1/124 \text{ kyr}^{-1}$, and $1/22.4 - 1/23.7 \simeq 1/405 \text{ kyr}^{-1}$ (Berger et al., 2005).

35 Milankovitch (1941) proposes that the glacial cycles are caused by summer insolation changes at high Northern latitudes (Fig. 1c), where ice sheets can widely expand. Boreal summer insolation has prominent periodicities on the 19–23.7-kyr climatic precession band and on the 41-kyr obliquity band, while it has negligible power near the 100-kyr band (Figs 1f and 1g, orange). Nevertheless, the dominant periodicity of glacial cycles is ∼100 kyr over the last 1 Myr (Fig. 1i, black); the 100 kyr problem (Imbrie et al., 1993; Paillard, 2001; Lisiecki, 2010). The climate system must thus exhibit some mechanism which

40 produces the ∼100-kyr periodicity, although the input powers concentrate in the ∼20-kyr and 41-kyr bands.

Previous studies link the ∼100-kyr glacial cycles with two or three obliquity cycles (Huybers and Wunsch, 2005; Bintanja and Van de Wal, 2008), four or five climatic precession cycles (Raymo, 1997; Ridgwell et al., 1999; Cheng et al., 2016), eccentricity cycles (Lisiecki, 2010; Rial, 1999) or combinations thereof (Huybers, 2011; Ganopolski and Calov, 2011; Parrenin and Paillard, 2012; Abe-Ouchi et al., 2013; Tzedakis et al., 2017). On a closer look, the ∼100-kyr peak in Fig. 1i locates near the

45 95-kyr periodicity where the eccentricity has a spectral peak (Fig. 1g, black), suggesting a possible influence of the eccentricity cycle on the glacial cycles (Rial, 1999). On the other hand, the strongest periodicity of the eccentricity, at 405 kyr over the last 1 Myr, is hardly apparent in the power spectral density (PSD) of the glacial cycles (Fig. 1i); the 400 kyr problem (Imbrie and Imbrie, 1980). Hence, the mechanism producing the 100-kyr periodicity would additionally have to involve a damping of the 405 kyr eccentricity periodicity.

50 Several types of mechanisms have been proposed to explain the ∼100-kyr cycles: threshold-based mechanisms (Raymo, 1997; Paillard, 1998; Abe-Ouchi et al., 2013; Tzedakis et al., 2017), various types of resonance or amplification of the forcing (Hagelberg et al., 1991; Le Treut and Ghil, 1983; Rial, 1999; Daruka and Ditlevsen, 2016; Verbitsky et al., 2018; Benzi et al., 1982; Nicolis, 1981; Matteucci, 1989; Ditlevsen, 2010; Pelletier, 2003; Bosio et al., 2022), as well as synchronization of internal oscillations (Saltzman et al., 1984; Gildor and Tziperman, 2000; Rial, 2004; Ashkenazy and Tziperman, 2004; Lisiecki,

55 2010; De Saedeleer et al., 2013; Crucifix, 2013; Ashwin and Ditlevsen, 2015; Mitsui et al., 2015; Nyman and Ditlevsen, 2019).

Synchronization (or, synonymously, *frequency-entrainment*) requires internal self-sustained oscillations in the absence of external forcing, which are going to be synchronized to the external forcing (Pikovsky et al., 2003). When synchronization is achieved, the frequency of glacial cycles is entrained at one of the astronomical frequencies, a subharmonic, or a combination tone thereof (see Appendix A for details). In synchronization theory, the external forcing is commonly assumed to be compara-

60 bly weak, so that the internal self-sustained oscillations are not drastically altered by the forcing (Pikovsky et al., 2003). Even if the forcing is weak, synchronization occurs if the frequency of internal oscillations is not too far away from the frequency of the external forcing (the principle of synchronization). Therefore, if the ∼100-kyr cycles are generated consistently with the synchronization mechanism, the system is expected to exhibit unforced oscillations of a similar time scale.

On the other hand, nonlinear response mechanisms, including several proposed threshold mechanisms as well as subharmonic responses (one response against multiple cycles of forcing), attempt to explain the $\sim$100-kyr periodicity without assuming underlying self-sustained oscillations (Abe-Ouchi et al., 2013; Daruka and Ditlevsen, 2016; Verbitsky et al., 2018). Thus, in principle, synchronization and nonlinear responses are distinguished with respect to the existence of internal self-sustained oscillations. However, as revisited in Section 5 below, their distinction could be subtle if the external forcing is comparatively large or if noise-induced oscillations, which arise in excitable systems, are 'synchronised' to a periodic forcing (i.e., stochastic resonance) (Pikovsky et al., 2003).

In this study we report synchronization phenomena observed in glacial cycles simulated in the Earth system model of intermediate complexity (EMIC) CLIMBER-2 with a fully interacive carbon cycle (Willeit et al., 2019; Ganopolski and Brovkin, 2017). It has been previously shown that this mode can reproduce the characteristics of Quaternary glacial cycles including the MPT using slowly changing volcanic CO_2 outgassing and regolith cover (Willeit et al., 2019). So far various explanations have been proposed for the MPT such as a nonlinear ice-sheet response to a long-term cooling trend (Berger et al., 1999; Bintanja and Van de Wal, 2008) possibly due to a long-term decline of the atmospheric CO_2 concentration, an onset of a positive feedback between the glacial intensification and additional glacial CO_2 drawdown by dust-borne iron fertilization (Chalk et al., 2017), an activation of the sea ice switch mechanism (Gildor and Tziperman, 2000), a change in the East Antarctic ice sheet margin from land-based to marine-based (Raymo et al., 2006), and the gradual removal of regolith by glacial erosion and an exposure of high-friction crystalline bedrock (Clark and Pollard, 1998). On the other hand, some models capture the frequency change across the MPT without any changes in their internal parameters, suggesting that the MPT is caused, at least in part, by changes in the astronomical parameters (Imbrie et al., 2011; Watanabe et al., 2023). Thus the physical mechanism of the MPT is still actively debated (Berends et al., 2021; Ford and Chalk, 2020; Clark et al., 2021). The purpose of this study is not to re-examine the physical mechanisms leading to the MPT in CLIMBER-2, which is discussed in Willeit et al. (2019), but to show novel synchronization phenomena underlying glacial cycles simulated in the model.

The remainder of this article is organized as follows. Section 2 describes the data and the model setting. In Section 3, we show that CLIMBER-2 exhibits spontaneous oscillations in the absence of the astronomical forcing, supporting the view of synchronization; the lengthening of the time scale of internal oscillations leads to the change of the entrained frequency across the MPT. In Section 4, we show that the frequency entrainment at the $\sim$100-kyr power is achieved by cooperative action of climatic precession and obliquity forcing, via a novel nonlinear mechanism, which we term *vibration-enhanced synchronization*. Section 5 is devoted to summary and discussion. Several caveats to this work are also given.

2 Methods

2.1 $\delta^{18}O$ record

The benthic $\delta^{18}O$ stack record (LR04) (Lisiecki and Raymo, 2005) is used throughout this study as empirical ground truth. It should be noted that the frequency and the strength of each spectral peak can in principle be affected by the orbital tuning of the record; a conservative tuning strategy is taken for the LR04 $\delta^{18}O$ record. Investigating the chronology of the record is however

beyond the scope of this work. We assume that the frequency structure of the LR04 record is basically correct including the observed dominance of 95-kyr periodicity over the last 1 Myr (Fig. 1i). The 95-kyr spectral peak is indeed observed in both orbitally tuned and untuned $\delta^{18}O$ records, although it is slightly subdued in untuned records (Rial, 1999). The conclusions are
100   derived from model simulations that are not subject to possible circular reasoning due to the orbital tuning.

2.2   CLIMBER-2 model and setting

Our study bases on an Earth System Model of Intermediate Complexity (EMIC) called CLIMBER-2 (Petoukhov et al., 2000; Ganopolski et al., 2001, 2010; Ganopolski and Calov, 2011; Brovkin et al., 2012; Ganopolski and Brovkin, 2017; Willeit et al., 2019). It couples atmosphere, ocean, vegetation, global carbon, and dust models, and a three-dimensional thermomechanical
105   ice sheet model (Greve, 1997). This is the most comprehensive EMIC that, thanks to its exceptional simulation speed, still allows to perform the analysis required here, with a large number of Myr-scale simulations. The CLIMBER-2 in this study is the same version used by Willeit et al. (2019). They simulated the glacial cycles over the last 3 Myr, assuming scenarios about a long-term reduction in the volcanic-CO_2 outgassing rate and gradual changes of ice-sheet substratum from regolith to hard-friction crystalline bedrock by glacial erosion (Fig. 1e), which we call the background condition (BC). Older BCs are
110   characterized by higher volcanic CO_2 outgassing rate and wider area of regolith (the continents are assumed to be fully covered by regolith at 3 Myr BP). The present-day BC consists of the volcanic outgassing rate of 5.3 Tmol C/yr and the distribution of regolith cover based on present-day observations, in which large parts of North America and Scandinavia are characterized by exposed crystalline bedrock. These temporal changes in BC underlie the simulated MPT accompanying the dynamical change from 41-kyr to ∼100-kyr glacial cycles (Willeit et al., 2019). The simulated $\delta^{18}O$ (Fig. 1d, magenta) under the optimal scenario
115   (Willeit et al., 2019) (Fig. 1e) is shown over the last 2 Myr.

While we basically follow the previous model settings (Willeit et al., 2019), we here perform 1-Myr-scale simulations with temporarily fixed BCs, which are values taken from the optimal scenario at a specific time (Fig. 1e). Fixed BCs are not optimal for simulating observations faithfully but may make the interpretation of results easier. All simulations have been initialized using the same initial state, corresponding to an interglacial state obtained from a transient simulation of the last four glacial
120   cycles, but with an ice-free Greenland (Willeit et al., 2019). However, the model runs were started from different points in time between 1.1 and 1.2 Myr BP for simulations over 1–0 Myr BP (between 2.1 and 2.2 Myr BP for simulations over 2–1 Myr BP) and thus from different initial astronomical configurations. The initial 100–200 kyr data is removed from power spectral analyses (Appendix C).

In order to understand the effects of different astronomical parameters, we conduct a series of sensitivity experiments. In
125   each, the CLIMBER-2 is simulated for a fixed astronomical configuration or forced by an hypothetical astronomical forcing. In the latter case, the amplitudes of eccentricity or obliquity variations are scaled up or down. A single 1.1-Myr simulation run takes roughly 14 days on a CPU core on the PIK HPC cluster (Xeon E5-2667v3 8C 3.2GHz, 335 Infiniband FDR14).

3   Unforced self-sustained oscillations and synchronization

3.1   Reference experiments

130   We first simulate glacial cycles under the true astronomical forcing (Laskar et al., 2004), which serves as reference simulation for further experiments.

Under fixed background conditions (BC) of volcanic CO_2 outgassing rate and regolith cover at their 1.6-Myr-BP values, which we assume representative for the BC over the period from 2 Myr to 1 Myr BP, CLIMBER-2 simulates $\delta^{18}O$ series similar to the observed record (Lisiecki and Raymo, 2005) (Fig. 2b). The dominant spectral power at the 41-kyr obliquity band

135   is reproduced (Fig. 2b). Simulated powers at precession bands are stronger than in the record but still minor.

With BC fixed at their present-day values, the model exhibits glacial cycles with strong ~100-kyr periodicity over the period from 1 Myr BP to present (Fig. 2d). Simulated glacial cycles depend on the initial times at which the simulations are started; there are time epochs in which trajectories starting from different initial conditions get close to each other, while the trajectories diverge in some other epochs. That is, the simulated glacial cycles are partially synchronized by the astronomical

140   forcing. This type of temporal instability typically appears in dynamical systems driven by quasiperiodic forcing like the astronomical forcing (Mitsui and Crucifix, 2016; Mitsui and Aihara, 2014; Riechers et al., 2022). Accordingly the PSD also depends on initial times. Nevertheless, a large fraction of spectral power is attracted by the periodicities of the eccentricity at 95 kyr, 124 kyr, and 405 kyr (Fig. 2d).

The 95-kyr power tends to be strongest statistically, although it is weaker than that of the observed record (Fig. S2 for blow

145   up). On the other hand, simulated 405 and 124-kyr powers are stronger than those in the record. These discrepancies are partly due to the fact that, in the present experimental setting, the model fails to simulate the deglaciation around ~430 kyr BP. Indeed CLIMBER-2 is able to produce a stronger ~100-kyr power and substantially weaker 405-kyr power if the simulation is started from an interglacial level at 410 kyr BP (Fig. S3). Also the 95-kyr spectral peak could potentially be accentuated in proxy records by the orbital tuning (Rial, 1999). Overall, we note that both the 41-kyr power in the pre-MPT experiment and the

150   95-kyr power in the post-MPT experiment are reproduced well, given the complexity of the model.

3.2   Internal self-sustained oscillations

Previous work demonstrated that the MPT simulated in CLIMBER-2 cannot be produced by changes in the astronomical forcing alone (Willeit et al., 2019). Indeed, CLIMBER-2 simulates 41-kyr cycles under the 1 Myr-to-present astronomical forcing when the BC at 1.6 Myr BP is used, and it simulates ~100-kyr cycles under the 2 Myr-to-1 Myr astronomical forcing if

155   the present-day BC is used (Fig. S4). These results provide further evidence that changes in the internal dynamics of the Earth system are necessary to explain the MPT.

The internal dynamics is investigated with unforced simulations for fixed orbital configurations. The configuration with zero eccentricity $e = 0$ and mean obliquity $\varepsilon = 23.34°$ effectively gives an average seasonal insolation change (Fig. S5). This is reasonable since any insolation curve for a season and a latitude is well approximated by a linear combination of the obliq-

160   uity ε, climatic precessions $e\sin\omega$ and co-precession $e\cos\omega$ (Imbrie and Imbrie, 1980). For this fixed orbital configuration,
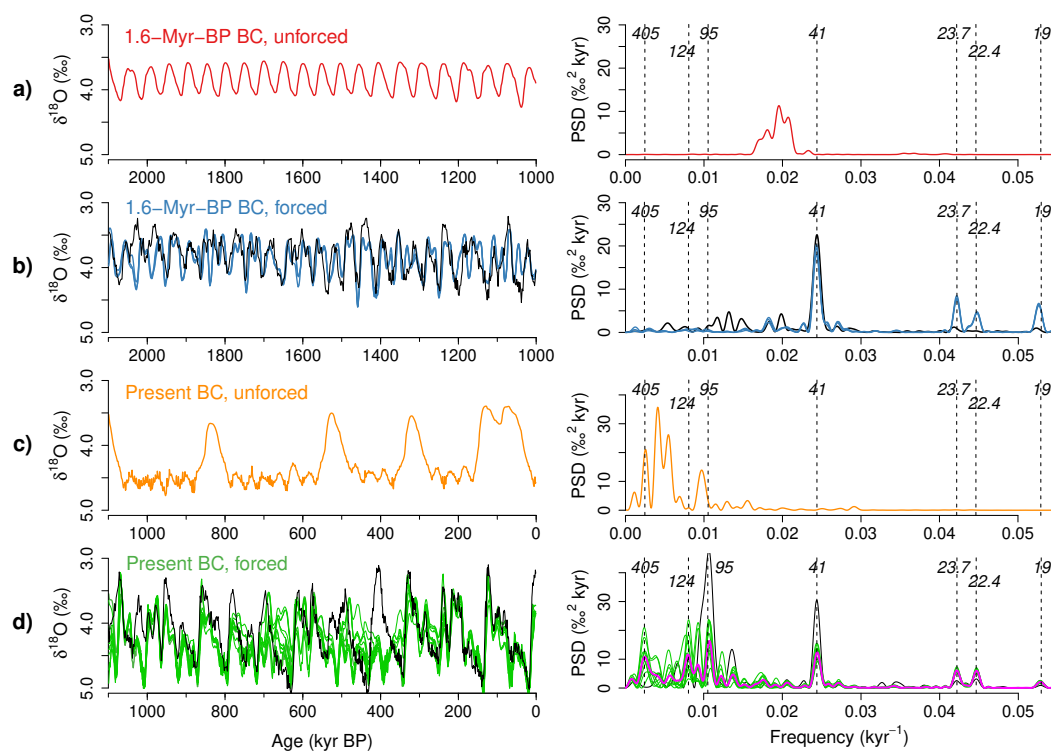
Figure 2. Comparison between unforced and forced simulations. (a) Unforced simulation of δ^{18}O under 1.6-Myr-BP background conditions (BC) and fixed orbital configuration with zero eccentricity and mean obliquity (left). The corresponding power spectral density (PSD) over 2-1 Myr BP (right). (b) Same as (a) but for true astronomical forcing (blue). The results for three slightly different initial times (i.e., initial orbital configurations) are shown. The black line corresponds to the δ^{18}O record (Lisiecki and Raymo, 2005). (c) Unforced simulations under 0-Myr-BP BC and fixed orbital configuration with zero eccentricity and mean obliquity. (d) Same as (c) but for true astronomical forcing (green). The results for ten slightly different initial times (i.e., initial orbital configurations) are shown. The magenta line in the right panel is the ensemble average of the ten PSDs. The black line corresponds to the δ^{18}O record (Lisiecki and Raymo, 2005).
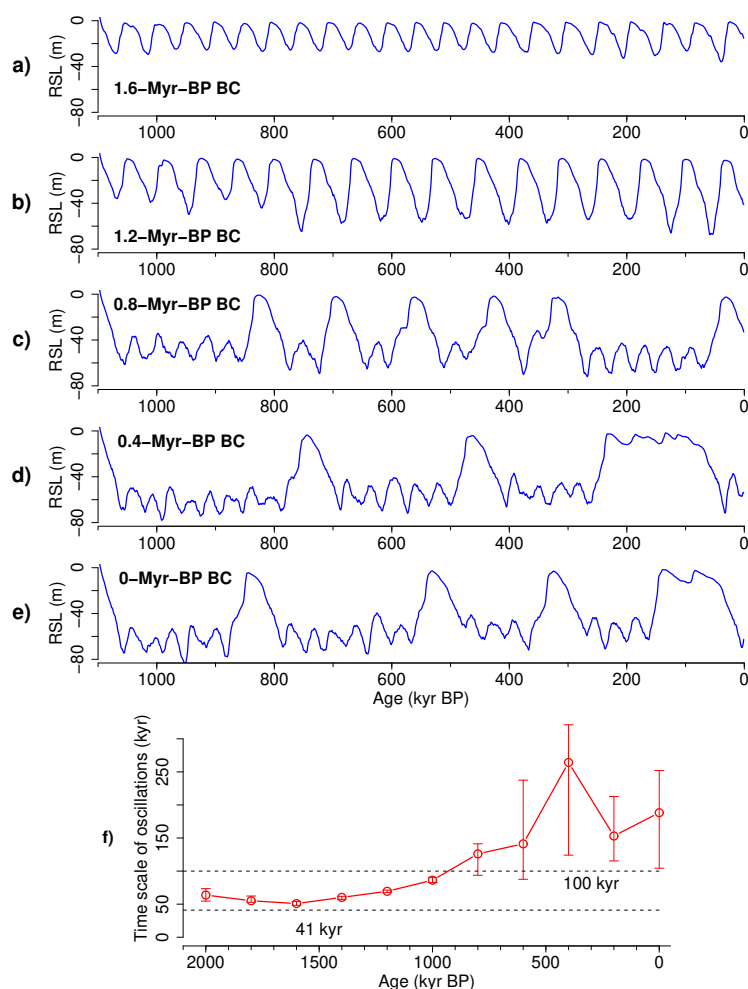
Figure 3. Gradual increase of the time scale of internal oscillations, inferred from simulations with fixed orbital configuration (zero eccentricity and mean obliquity). Simulated relative sea level (RSL) for different background conditions (BC) of volcanic CO_2 outgassing rate and regolith cover corresponding to (a) 1.6 Myr, (b) 1.2 Myr, (c) 0.8 Myr, (d) 0.4 Myr, and (e) 0 Myr BP. (f) The internal time scale as a function of age, from which the BC used for the simulation is taken. The time scale is derived from the PSD of the corresponding time series over 1000 kyr BP to present. The circles denote the medians and the vertical bars show the interquartile range. The horizontal dashed lines indicate 41 kyr and 100 kyr for reference.

CLIMBER-2 exhibits self-sustained oscillations with time scales dependent on the BCs. Quasi-regular self-sustained oscillations with periodicity around 50 kyr arise for BC fixed at their values of 1.6 Myr BP (Fig. 2a). Less regular self-sustained oscillations with a time scale of a few hundred kyr arise for present-day BC (Fig. 2c). Overall, the time scale of self-sustained oscillations gradually increases when moving from $\sim$1.5-Myr-BP BC to $\sim$0.5-Myr-BP BC (Fig. 3). This increase of the inter-

165 nal time scale is accompanied by an increase in the amplitude of the oscillations (i.e., intensification of glacials). However in these unforced simulations for $e = 0$ and $\varepsilon = 23.34°$, the sea level variations are limited to $\sim$80 m (Fig. 3), which is smaller than that of the forced case ($\sim$120 m). Similar lengthening of internal time scales occurs also for the present-day orbital configuration (Fig. S6) and for the orbital configuration at the Last Glacial Maximum (21 kyr BP) (Fig. S7). In those cases, much larger ($\sim$250 m) and much longer (half-Myr scale) oscillations are observed for the post-MPT BCs.

170 The self-sustained oscillations of CLIMBER-2 found here are generated by various feedback processes described in previous studies (Ganopolski et al., 2010; Ganopolski and Calov, 2011; Brovkin et al., 2012; Ganopolski and Brovkin, 2017). Among others, the glaciogenic dust feedback and the carbon cycle feedback play a key role. Indeed, if the atmospheric CO_2 concentration is fixed to a constant value and if the glaciogenic dust feedback is switched off, the spontaneous oscillations cease or, even if some fluctuations remain, their amplitudes are reduced (Fig. S8).

175 In the unforced simulation for the BC at their 1.6-Myr-BP values, $e = 0$ and $\varepsilon = 23.34°$ (Fig. 4), ice sheets nucleate and then grow facilitated by the ice albedo feedback. However, once the sea level reaches around -30 m, the ice sheets rapidly shrink due to an abrupt increase of glaciogenic dust deposition over the Northern Hemisphere ice sheets (Fig. 4b), which reduces the ice albedo and enhances ablation (Ganopolski et al., 2010; Ganopolski and Calov, 2011). The glaciogenic dust emission continues throughout the deglaciation. In the unforced simulation with 1.6-Myr BC, the period of self-sustained oscillations

180 ($\sim$50 kyr) is primarily set by ice sheet dynamics and the glaciogenic dust feedback. The carbon cycle feedback slightly modifies the oscillation amplitude but does not affect the oscillation period significantly. Indeed in the unforced simulations with fixed atmospheric CO_2 concentrations over 180–300 ppm and the 1.6-Myr-BP BC (Fig. 5, left), the period of self-sustained oscillations stably remains in a narrow range between 45 kyr and 60 kyr.

In the unforced simulation with the present-day BC, $e = 0$ and $\varepsilon = 23.34°$ (Fig. 6), the carbon cycle feedbacks play a crucial

185 role in setting the time scale and the amplitude of spontaneous oscillations. Starting from the sea level of zero, the ice sheets nucleate and grow in association with a decrease in the atmospheric CO_2 (Figs 6a and 6d). As the sea level decreases below -50 m, enhanced dust deposition in the Southern Ocean induces a further rapid reduction of CO_2 via the iron fertilization effect, which causes a further ice volume increase (Figs 6a and 6b). However, then a sudden increase of glaciogenic dust deposition over the Northern Hemisphere ice sheets interrupts their growths by reducing albedo and enhancing ablation (Figs 6a and 6c).

190 These counteracting effects keep the sea level around -80 to -50 m for one or two hundred kyr, but finally the ice sheets retreat with the help of the glaciogenic dust deposition sustained during the deglaciation. The simulations with fixed atmospheric CO_2 concentration (Fig. 5, right) suggest that the glacial ice sheets are more stable (that is, the glacial duration becomes longer) if the prescribed CO_2 concentration is lower (cf. Willeit et al. (2019)). In sum, the hundred-kyr-scale periodicity of self-sustained oscillations (Fig. 6) emerges from the combined effect of ice sheet dynamics, glaciogenic dust and carbon cycle feedback.

195 There is a little warming trend superimposed on the self-sustained oscillations (Fig. 6) due to a long-term CO_2 increase caused
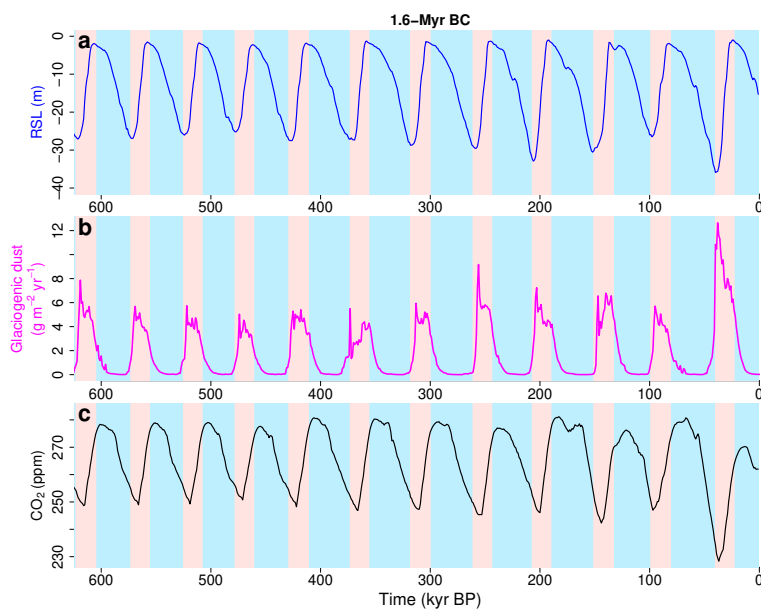
Figure 4. Self-sustained oscillations for the background condition (regolith cover and volcanic outgassing rate) at 1.6 Myr BP and a fixed orbital configuration ($e = 0$ and $\varepsilon = 23.34°$). (a) Relative sea level (RSL). (b) Glaciogenic dust deposition rate. The mean value at ($100°$E, $45°$N) and ($100°$E, $55°$N). (c) Atmospheric CO_2 concentration. The oscillation period is about 50 kyr.

by a small imbalance in carbon fluxes, but the self-sustained oscillations persist over the periods that simulations are conducted (at least beyond 1.5 Myr).

3.3 Frequency entrainment

It remains to be explained how the change in the internal time scale leads to the observed frequency change across the MPT.

200 If we compare the spectra of forced simulations with those of corresponding unforced ones (Fig. 2), we find that the spectral powers of forced simulations are entrained at one or few astronomical frequencies near the frequency of internal self-sustained oscillations. The theory of synchronization (Pikovsky et al., 2003) may provide a general explanation for these observations. In essence, frequency entrainment (i.e., synchronization) tends to occur near the internal frequency as long as the external forcing is moderate (Fig. S1 and Appendix A).

205 Consistently with synchronization theory, the oscillations before the MPT are entrained by the 41-kyr obliquity cycles, due to the proximity of the internal periodicity (around 50 kyr) to the 41 kyr-oblquity periodicity (Figs 2a and 2b). The oscillations after the MPT are entrained by the eccentricity periodicities at 95, 124, and 405 kyr because the several-hundred-kyr time scales of internal oscillations for post-MPT BCs are closer to those eccentricity periodicities than to the much smaller obliquity periodicity (Figs 2c and 2d). Reflecting temporarily desynchronized epochs in the simulated glacial cycles after the MPT, the

210 magnitudes of the 95-, 124- and 405-kyr-band powers depend on the realizations of simulated sequences. If the ensemble
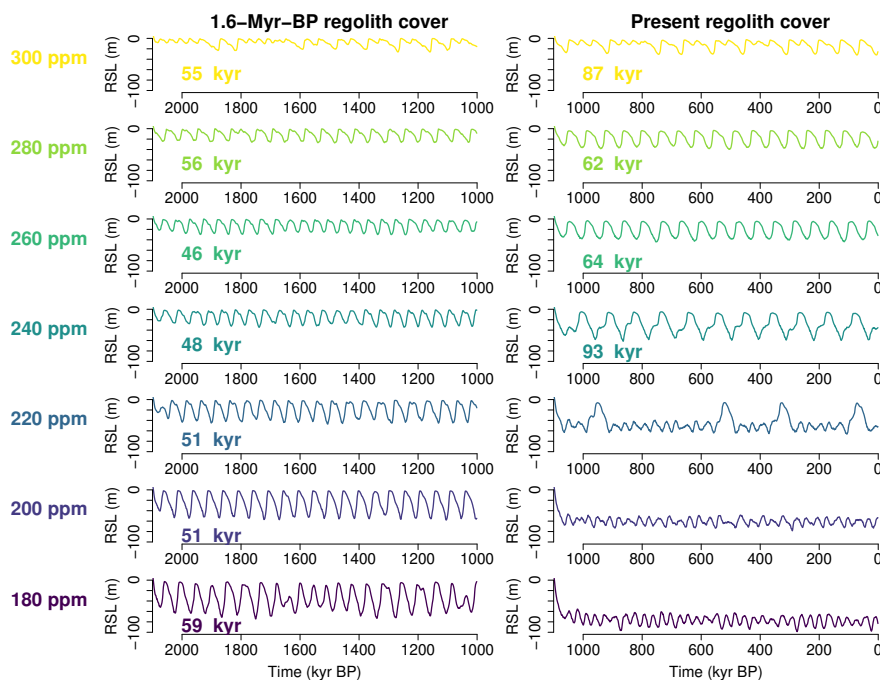
Figure 5. Relative sea level (RSL) simulated by CLIMBER-2 for fixed atmospheric CO_2 concentration and a fixed orbital configuration ($e = 0$ and $\varepsilon = 23.34°$): (Left column) Simulations with 1.6-Myr-BP regolith cover. (Right column) Those with the present regolith cover. All feedback processes except for the carbon cycle feedback are active. The number in each panel is the mean period of oscillations that reaches the sea level of 0 m.

average is taken for the spectra (from 27 simulations), the 95-kyr-band power is the strongest (Fig. S2b). For some realizations, a noticeable peak arises at 107-kyr periodicity (Fig. S2), which may be interpreted as a higher-order combination tone of 95-kyr and 405-kyr eccentricity periodicities ($1/107 \simeq 1/95 - 1/(2 \times 405)$) (Rial (1999) and Appendix A).

The frequency-entrainment at the eccentricity frequencies does not result from the eccentricity forcing itself but results from
215 the climatic precession forcing $e \sin\omega$ ($e \cos\omega$), whose amplitude is modulated by the eccentricity cycles. As shown in Fig. B1 in Appendix B, the deglaciations occur near peaks of climatic precession (i.e., boreal summer insolation peaks) in rising or high phases of eccentricity (Raymo, 1997; Ridgwell et al., 1999; Ganopolski and Calov, 2011; Abe-Ouchi et al., 2013).

Given that the eccentricity has the strongest power at 405-kyr over the last 1 Myr, it is unclear why – and actually rather surprising that – the internal oscillations with a time scale of a few hundred kyr are entrained most strongly by the 95-kyr
220 periodicity, and not by 405 kyr. In what follows we show that the 41-kyr obliquity variations play a crucial role in synchronising the climate system to the 95-kyr rather than the 405-kyr periodicity, via a new nonlinear phenomenon that we term vibration-enhanced synchronization.
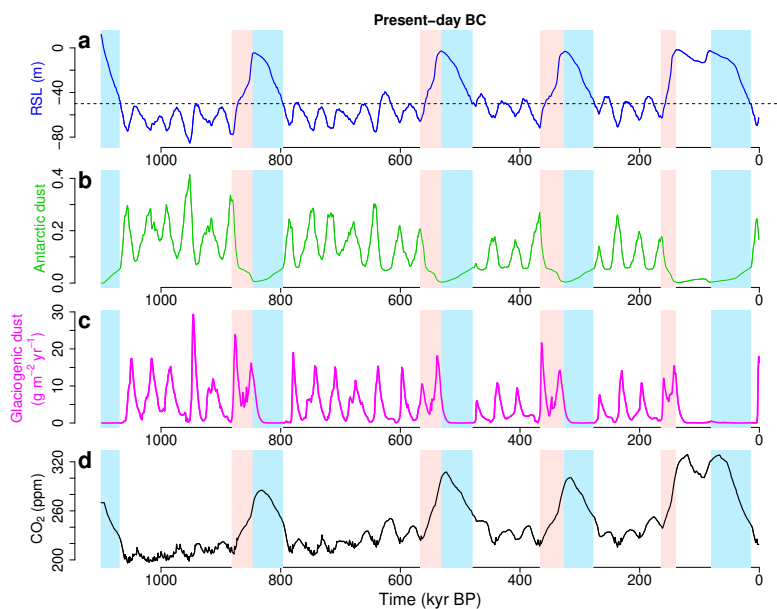
Figure 6. Self-sustained oscillations for the present background condition (regolith cover and volcanic outgassing rate) and fixed orbital configuration $e = 0$ and $\varepsilon = 23.34°$: (a) Relative sea level (RSL). The horizontal dashed line indicates the RSL of -50 m, below which the dust-borne iron fertilization of the Southern Ocean is enhanced in the model. (b) Antarctic dust deposition in relative unit as a proxy for the iron flux over the Southern Ocean. (c) Glaciogenic dust deposition rate. The mean value at $(100°E, 45°N)$ and $(100°E, 55°N)$. (d) Atmospheric CO_2 concentration. The mean periodicity is about 250 kyr.

4 Cooperative effect of the changes of astronomical elements

In order to investigate the respective roles of climatic precession and obliquity forcing in producing the dominant 41-kyr and
225 $\sim$100-kyr periodicities before and after the MPT, we conduct two sets of sensitivity experiments with BC fixed at pre-MPT (i.e., 1.6 Myr BP) and at post-MPT (i.e., present-day) values, respectively. First, we run CLIMBER-2 simulations with the actual obliquity $\varepsilon(t)$ and a scaled eccentricity $Ae(t)$, with $0 \leq A \leq 2.5$. The climatic precession is accordingly scaled (i.e., $Ae\sin\omega$), but its phase is the same as the real variation. Second, we run the model with the true eccentricity and climatic precession, but with scaled obliquity $\varepsilon'(t) = 23.34° + B(\varepsilon(t) - 23.34°)$, with $0 \leq B \leq 2.5$. The real-world forcing corresponds to $A = 1$
230 and $B = 1$. The PSDs are calculated for the simulated $\delta^{18}O$ time series for varying A and B. To get clearer insights about the changes in PSDs, we investigate the ensemble-averaged normalized PSD and the ensemble-averaged relative band strength for changing combinations of A and B (see Appendix C).
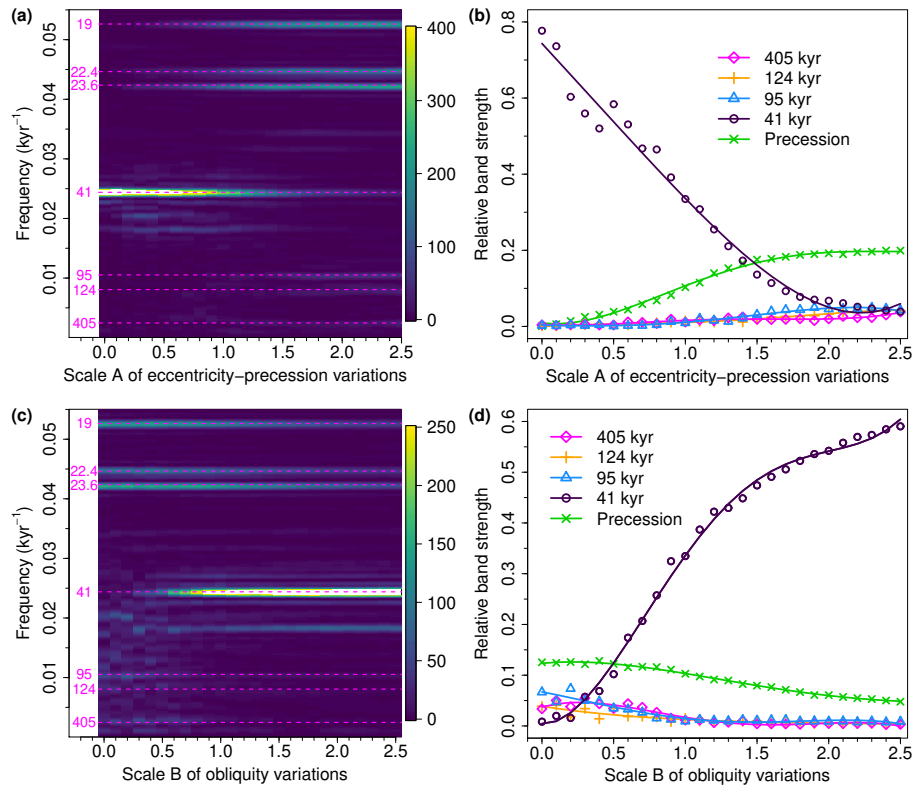
Figure 7. Sensitivity experiments with respect to the astronomical forcing under pre-MPT (1.6 Myr BP) background condition. (a) Averaged normalized power spectral density (PSD) of three CLIMBER-2 simulations as a function of the scale A of the eccentricity and climatic precession. The horizontal dashed lines (magenta) and associated numbers indicate the major astronomical frequencies (corresponding to periodicities at 405, 124, 95 and 41 kyr). (b) Relative band strengths P_{405}, P_{124}, P_{95}, P_{41} and $P_{\text{precession}}$ as functions of A, obtained from the PSD in (a); cf. Appendix C. The lines are forth-order polynomial fits to the data points. (c) Averaged normalized PSD of the CLIMBER-2 simulations as a function of the scale B of the obliquity. (d) Relative band strengths as functions of B, obtained from the PSD in (c).
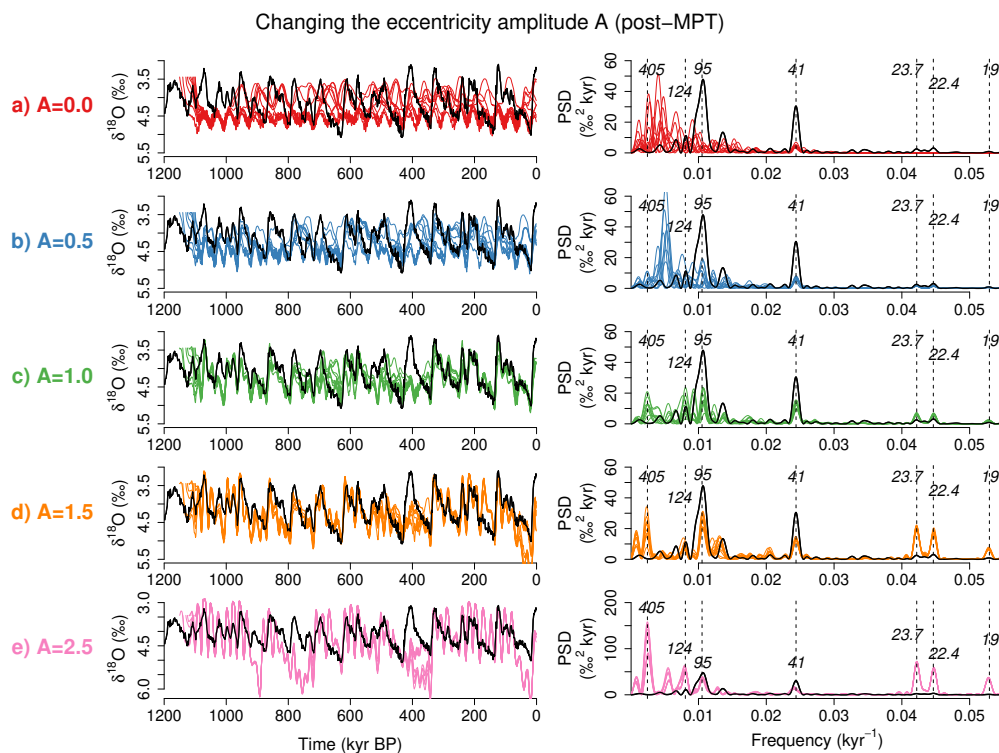
4.1 Pre-MPT background conditions

First, the scale A of eccentricity-climatic precession forcing is changed while keeping the real obliquity forcing. As long as the
scale A of eccentricity-climatic precession forcing is moderate ($A \lesssim 1.5$), the 41-kyr power dominates; for $A \gtrsim 1.5$ the mean
precession-band power dominates the 41-kyr-band power (Figs S9, 7a and 7b).

Second, we change the scale B of obliquity variations while keeping the actual eccentricity-precession forcing (Figs S10,
7c and 7d). If the obliquity forcing is absent or very weak ($B \lesssim 0.3$), the sequences of simulated glacial cycles starting from
different initial conditions are not fully synchronized with each other (Fig. S10a for $B = 0$) and exhibit complex oscillations
having dominant powers at the precession bands (Figs S10a, 7c and 7d). However, if the obliquity forcing is strong enough
($B \gtrsim 0.5$), the sequences of simulated glacial cycles starting from different initial conditions are synchronized well with each
other and with the 41-kyr obliquity cycles (Fig. S10). The 41-kyr-band power increases rather rapidly over $0.5 \lesssim B \lesssim 1.2$,
exceeding the average precession-band power (Fig. 7d). This nonlinear increase of the 41-kyr power with B can be partly
explained as a synchronization. However, the amplitude of simulated glacial-cycle oscillations moderately increases as the
forcing amplitudes A and B increase (Figs S9 and S10). This is the aspect of linear response.

4.2 Post-MPT background conditions

First, the eccentricity–climatic precession is scaled while keeping the actual obliquity forcing (Figs 8, 10a and 10b). In the
absence of eccentricity–climatic precession change ($A = 0$), the obliquity forcing alone cannot constrain the sequence of
glacial cycles, and the PSDs are not substantially different from those of internal oscillations, having largest powers in between
400 and 100-kyr band (Fig. 8a). If the scale A of eccentricity is increased up to around $A = 1$, the oscillations are roughly
synchronized to the 95-kyr periodicty, which is strongest statistically, although also the 124-kyr and 405-kyr band may receive
a noticeable fraction of the the spectral power, depending on initial conditions (Figs 8c, 10a, 10b and S1). For $A > 1.8$, the 405-
kyr band receives the maximum strength (Figs 10a and 10b). For the extreme case $A = 2.5$, huge ice sheets appear near every
400 kyr eccentricity minimum (Fig. 8e). The system achieves a synchronized state with prominent ∼100-kyr periodicity for
a realistic scale of the eccentricity–climatic precession forcing ($A \approx 1$), and the dynamics shifts toward a nonlinear resonance
mode with the 405-kyr eccentricity cycles for much larger A. It is worth mentioning that the relative strength of the 41-kyr
power is largest near $A = 1$ (Fig. 10b).

Second, the scale B of obliquity variations is varied while we keep the actual eccentricity–climatic precession forcing (Figs 9,
10c and 10d). In the absence of obliquity forcing ($B = 0$), glacial-interglacial cycles are likely to occur when the eccentricity
is large, giving rise to a roughly 400-kyr periodicity (Fig. 9a); the 95-kyr mode still exists, while it is weaker than the 405-kyr
mode. As B increases, the 405-kyr band power is suppressed and the 41-kyr-band power increases. Statistically, the 95-kyr
power becomes strongest in the range $0.7 \lesssim B \lesssim 1.2$ (Figs 10c and 10d). This is nontrivial because the dominance of 95-
kyr periodicity is enabled by the 41-kyr obliquity forcing, which is directly related to neither 95-kyr nor 405-kyr periodicity.
We call this novel nonlinear mechanism *vibration-enhanced synchronization*. It may be seen as a deterministic analogue of
noise-enhanced synchronization of chaotic oscillations to a weak periodic signal (Zhou et al., 2003), and of the noise-induced
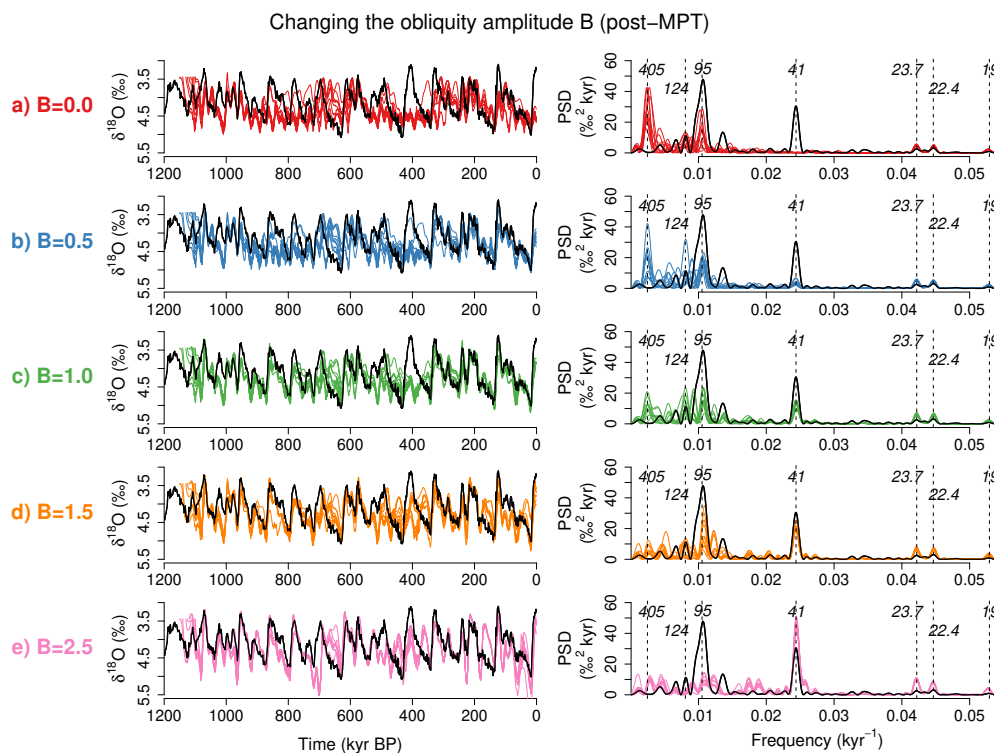
Figure 8. Sensitivity experiments changing the scale A of the eccentricity (Laskar et al., 2004) (and hence of climatic precession) under post-MPT background conditions (see text). Ten simulated $\delta^{18}O$ time series starting from different initial times (i.e., different orbital configurations) are shown for different values of A on the left of (a) to (e). The black line is the LR04 $\delta^{18}O$ record (Lisiecki and Raymo, 2005). The corresponding power spectral densities (PSD) are shown on the right. The dashed vertical lines and italic numbers indicate the positions of major astronomical frequencies and their periods (Laskar et al., 2004). For A smaller than the realistic values $A = 1$, variability at time scales of several hundred kyr dominates. Near the realistic value $A = 1$, the glacial cycles synchronize to the 95-kyr eccentricity cycle. For A much larger than 1, the system resonates with the 405-kyr eccentricity cycles.

entrainment of human brain waves (Mori and Kai, 2002). It has also an analogy to stochastic resonance (Benzi et al., 1982; Nicolis, 1981; Matteucci, 1989; Ditlevsen, 2010), to coherence resonance (Pelletier, 2003; Bosio et al., 2022) and to vibrational resonance (Landa and McClintock, 2000) in the sense that apparently-irrelevant high-frequency variability with a suitable amplitude can amplify the response of the system to a slow forcing.

5 Summary and discussion

We have reported synchronization phenomena in the glacial cycles simulated in the Earth system model of intermediate complexity CLIMBER-2 (Willeit et al., 2019; Ganopolski and Brovkin, 2017), and have explained the rhythms of simulated glacial cycles from the perspective of the synchronization principle. We have found that when fixing astronomical parameters at their

Figure 9. Sensitivity experiments changing the scale B of the obliquity (Laskar et al., 2004) under the post-MPT background condition (see text). Ten simulated $\delta^{18}O$ series starting from different initial times (i.e., different orbital configurations) are shown for different values of A on the left of (a) to (e). The black line is the LR04 $\delta^{18}O$ record (Lisiecki and Raymo, 2005). The corresponding power spectral densities (PSD) are shown on the right. The dashed vertical lines and italic numbers indicate the positions of major astronomical frequencies and their periods (Laskar et al., 2004). The increase in the scale B of the obliquity variations reduces the 405-kyr power and makes the 95-kyr power dominate – the phenomenon of vibration-enhanced synchronization.

reasonable averages, the model exhibits self-sustained oscillations of periodicities around 50 kyr under pre-MPT background
275   conditions regarding volcanic CO_2 outgassing rate and the regolith cover. Under post-MPT background conditions, the un-
forced model exhibits spontaneous oscillations at time scales of a few hundred kyr. The glaciogenic dust feedback and the
carbon cycle feedback play key roles in the self-sustained oscillations. Before the MPT, the glacial cycles synchronize with the
41-kyr obliquity cycles since the internal oscillations have periodicity ($\sim$50 kyr) relatively close to 41 kyr. This follows the uni-
versal principle of synchronization: frequency-entrainment occurs if the frequency of internal self-sustained oscillations is in a
280   neighbourhood of the frequency of external forcing (Pikovsky et al., 2003). After the MPT the time scale of internal oscillations
becomes too long to follow the 41-kyr obliquity cycle, and the glacial cycles synchronize with the $\sim$100-kyr eccentricity cycles
(statistically most likely at 95-kyr band). In this case, via vibration-enhanced synchronization, the 41-kyr obliquity variations
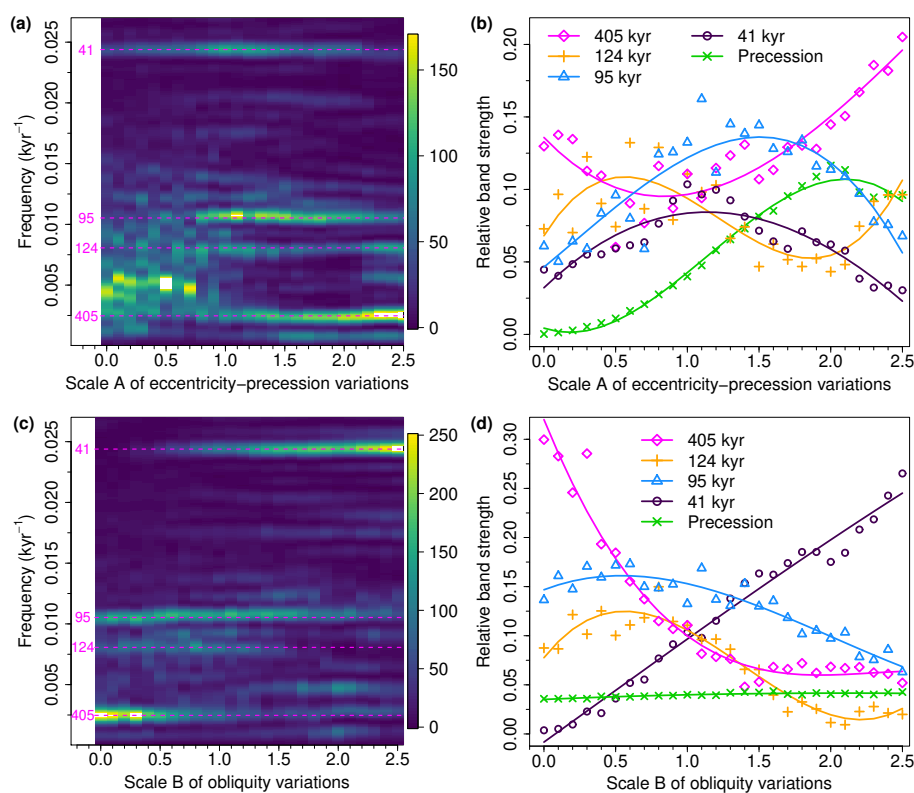
Figure 10. Sensitivity experiments with respect to the astronomical forcing under post-MPT background conditions. (a) Averaged normalized power spectral density (PSD) of ten CLIMBER-2 simulations as a function of the scale A of eccentricity and climatic precession. The horizontal dashed lines (magenta) and associated numbers indicate the major astronomical frequencies (corresponding to periodicities at 405, 124, 95 and 41 kyr). (b) Relative band strengths P_{405}, P_{124}, P_{95}, P_{41} and $P_{\text{precession}}$ as functions of A, obtained from the PSD in (a); cf. Appendix C. The lines are third-order polynomial fits to the data points. (c) Average PSD of the CLIMBER-2 simulations as a function of the scale B of the obliquity. (d) Relative band strengths as functions of B, obtained from the PSD in (c).
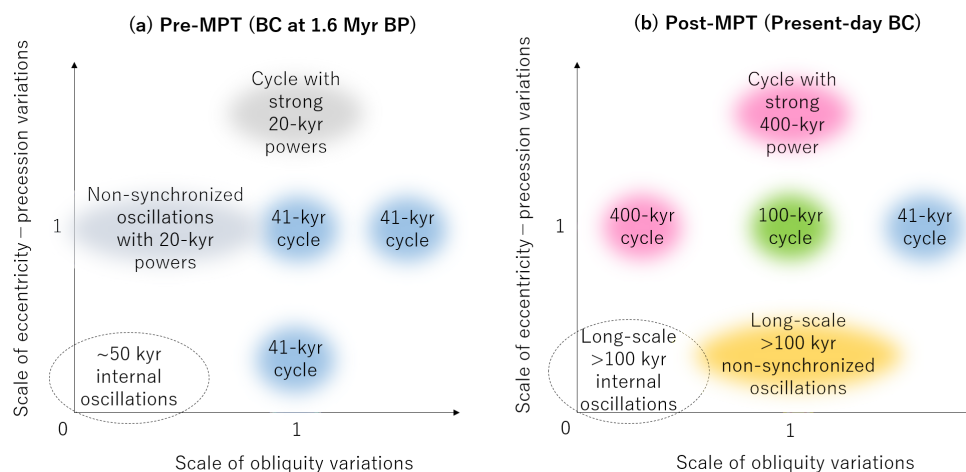
Figure 11. Summary diagrams illustrating various dynamical regimes realized by CLIMBER-2 for different scales of obliquity and eccentricity–climatic precession variations. (a) Results for the pre-MPT background conditions (BC), specifically 1.6-Myr-BP BC. The system exhibits internal oscillations of ∼50-kyr periodicity in the absence of forcings. For a realistic or smaller scale of eccentricity–precession forcing, the simulated glacial cycles synchronize to the 41-kyr obliquity forcing if the scale of obliquity variations is realistic or larger. (b) Results for the post-MPT BC, i.e., for present-day. The unforced system exhibits spontaneous oscillations of several hundred-kyr scale. The ∼100-kyr cycles occur only for realistic scales of obliquity and eccentricity–precession variations.

enable synchronization of oscillations at the ∼100-kyr eccentricity band (Figs 9, 10c and 10d). While the enhancement of the ∼100-kyr power by the 41-kyr obliquity forcing is consistent with previous modelling studies (Ganopolski and Calov, 2011; Abe-Ouchi et al., 2013), we have further shown that ∼100-kyr cycles become dominant only for a suitable amplitude range of obliquity variations (Fig. 11b).

Our results suggest that the MPT is due to the gradual increase in the period of the climate system's internal oscillations, leading to a transition from synchronizing to the 41-kyr obliquity to synchronizing to the ∼100-kyr eccentricity cycles. This is consistent with some previous studies (Nyman and Ditlevsen, 2019; Ashkenazy and Tziperman, 2004; Mitsui et al., 2015) and also coherent with the gradual increase in the deglaciation threshold (Paillard, 1998; Tzedakis et al., 2017; Berends et al., 2021; Legrain et al., 2023). Our theory is, however, incoherent with the Hopf bifurcation scenario, which assumes the onset of self-sustained (limit-cycle) oscillations around the timing of the MPT (Maasch and Saltzman, 1990; Crucifix, 2012), since the CLIMBER-2 simulations exhibit internal self-sustained oscillations before the MPT, and also because the internal frequency does not necessarily change across the Hopf bifurcation (Strogatz, 2018).

There are some caveats to our work. The CLIMBER-2 model in its present setting has some problems to simulate the deglaciation around 430 kyr BP, Termination V. The last deglaciation is incomplete, leaving the present interglacial colder than observed. The North American ice sheet nucleates at the preindustrial CO_2 level (Figs 5 and S8). Thus the present model setting, calibrated on several hundred-kyr glacial cycles, could be biased toward glacial states. Some parameters and parame-

terizations including the glaciogenic dust deposition process are only weakly constrained by empirical data, as mentioned in
300   Ganopolski et al. (2010). Therefore, it is important to examine in future work if similar self-sustained oscillations and synchro-
nization phenomena could be observed in a more recent version of CLIMBER-X (Willeit et al., 2022, 2023) as well as in other
comprehensive models.

Recently, Watanabe et al. (2023) have conducted similar sensitivity experiments changing the amplitudes of orbital variations
in the IcIES-MIROC model (Abe-Ouchi et al., 2013). In their simulations, if the amplitude of the climatic precession is reduced
305   to 20% (while the true obliquity is used), the dominance of the 41-kyr cycles is lost in the early Pleistocene, and glacial cycles
having a strong ∼100-kyr power arise. This strong sensitivity to the precession forcing in the 41-kyr cycles simulated by
the IcIES-MIROC model is contrasted with the weak sensitivity to the precession forcing in the 41-kyr cycles simulated by
CLIMBER-2 (Figs 7b and S9). This difference may be related to the presence of internal self-sustained oscillations with
periodicity close to 41-kyr in CLIMBER-2 (Fig. 2a) and the absence of the internal oscillations in IcIES-MIROC (Watanabe
310   et al., 2023). Nevertheless, our results with CLIMBER-2 do not contradict the observed influences of both climatic precession
and obliquity forcing on the early Pleistocene 41-kyr glacial cycles (Liautaud et al., 2020; Barker et al., 2022; Watanabe et al.,
2023). Indeed, the simulated sequence of glacial cycles and its spectra are close to those of the $\delta^{18}O$ record if the amplitude of
the climatic precession is realistic (Figs S11 and S12).

We have described the dominant rhythms of glacial cycles as the result of synchronization of internal oscillations to the
315   astronomical forcing. It should however be mentioned that, in the CLIMBER-2 simulations, the astronomical forcing not only
adjusts the frequency of glacial cycles, but also increases the amplitude of oscillations and makes the shape of the cycles
more asymmetric. In this sense the form of synchronization of glacial cycles slightly deviates from the prototypical notion of
synchronization, i.e., the frequency and phase adjustment of oscillators by *weak* forcing (Pikovsky et al., 2003). As stated in
Introduction, the distinction between synchronization and linear/nonlinear response can be subtle when the external forcing is
320   strong in comparison to the internal dynamics. Indeed, Le Treut and Ghil (1983) describe their simulated ∼100-kyr cycles as
nonlinear responses – more specifically, as nonlinear resonance – because in their model internal oscillations are smaller and
more rapid than forced, amplified oscillations. After the MPT, in agreement with the proxy records, CLIMBER-2 simulations
show dominant ∼100-kyr cycles, but they also exhibit more rapid oscillations, for example, over one precession cycle around
230 kyr BP and over two precession/one obliquity cycle around 600 kyr (Fig. B1). These rapid cycles may be seen as more
325   direct responses to the strong precession forcing associated with strong eccentricity at those time epochs, rather than as the
result of synchronization of hundred-kyr-scale spontaneous oscillations. Therefore, the glacial-interglacial cycles over the
last 1 Myr show different facets over the time: the synchronization of internal self-sustained oscillations with the ∼100-kyr
eccentricity cycles and the forced responses to the strong precession forcing associated with strong eccentricity (Imbrie et al.,
1992, 1993; Gildor and Tziperman, 2000; Lisiecki, 2010).

330   Based on the CLIMBER-2 simulations, we have suggested that the ∼100-kyr glacial cycles over the last 1 Myr are realized
by cooperative action of eccentricity–climatic precession forcing and obliquity forcing; this is only possible in a specific range
of the scales of orbital variations (Fig. 11). In the absence of the eccentricity–climatic precession forcing, the obliquity forcing
alone cannot synchronize the glacial cycles, and the time scales of oscillations are much larger than ∼100-kyr. The 95-kyr

Earth System
Dynamics
Discussions

Open Access

EGU

power dominates if the amplitude of climatic precession is realistic. However, the 405-kyr band becomes strongest for larger

335 amplitudes of eccentricity–climatic precession forcing and dominates in the absence of obliquity cycles. The increase in the

obliquity amplitude weakens the 405-kyr power and makes the 95-kyr power dominant as long as the obliquity amplitude is

realistic. If the obliquity amplitude is substantially larger than realistic values, the 41-kyr power simply dominates. Via the

phenomenon of *vibration-enhanced synchronization* the 41-kyr obliquity forcing thus helps the synchronization of the Earth's

climate system with the $\sim$100-kyr eccentricity cycles.

Appendix A: Frequency entrainment (synchronization)

When a self-sustained oscillator with frequency f_0 is subject to an external forcing with frequency f_e, the frequency of

oscillations under the forcing, f_r, can be entrained to f_e (i.e. $f_r = f_e$). This phenomenon is called *frequency-entrainment*

(or *frequency-locking*) and ubiquitously observed in natural or man-made oscillating systems (Pikovsky et al., 2003). This

frequency-entrainment occurs within a finite range of frequency detuning $f_e - f_0$, which is typically wider if the forcing is

345 stronger (Fig. S1). If the internal frequency f_0 is far away from the external frequency f_e but close to a simple harmonic

$(m/n)f_e$ $(m, n \in \mathbb{N})$, the higher-order $m : n$ synchronization can occur at $(m/n)f_e$ (i.e. $f_r = (m/n)f_e$). On the other hand the

higher-order synchronization has narrower entrainment region and is less likely than a lower-order one (Fig. S1). If the exter-

nal forcing has multiple frequencies (f_j, f_k and so on), the entrainment can occur at one of those frequencies, their harmonics

$(m/n)f_j$, or a combination tone (e.g., $(m/n)f_j \pm (l/n)f_k$) close to the internal frequency f_0.

Appendix B: Simulated deglaciations at climatic precession peaks

In CLIMBER-2 simulations over the last 1 Myr, the major deglaciations appear to be triggered by climatic precession peaks

corresponding to marked boreal summer insolation peaks in rising or high phases of eccentricity (Fig. B1), consistently with

some of previous proposals (Raymo, 1997; Ridgwell et al., 1999; Ganopolski and Calov, 2011; Abe-Ouchi et al., 2013).

In many cases, a high or above-average obliquity assists the deglaciation (cf. Tzedakis et al. (2017) and vibration-enhanced

355 synchronization proposed here). The frequency-entrainment at eccentricity frequencies occurs via the synchronization of a few

hundred-kyr self-sustained oscillations to the $\sim$100-kyr-scale amplitude modulation of climatic precession by the eccentricity

change.

Appendix C: Power spectral density

The power spectral densities (PSD) $S(f)$ of different time series are estimated via periodograms (Bloomfield, 2004), which

360 are computed with the R-function `spec.pgram` (R Core Team, 2020). In particular when we focus on the relative strength

of spectral peaks, we use the normalized PSD, defined as $S^N(f) = S(f)/\int_0^\infty S(f)df$. A split cosine bell taper is applied

to 10% of the data at the beginning and end of the time series in order to minimize the effect of the discontinuity between

the beginning and end of the time series (Bloomfield, 2004). All time series are padded with zeros so that their length is

Earth System
Dynamics
Discussions
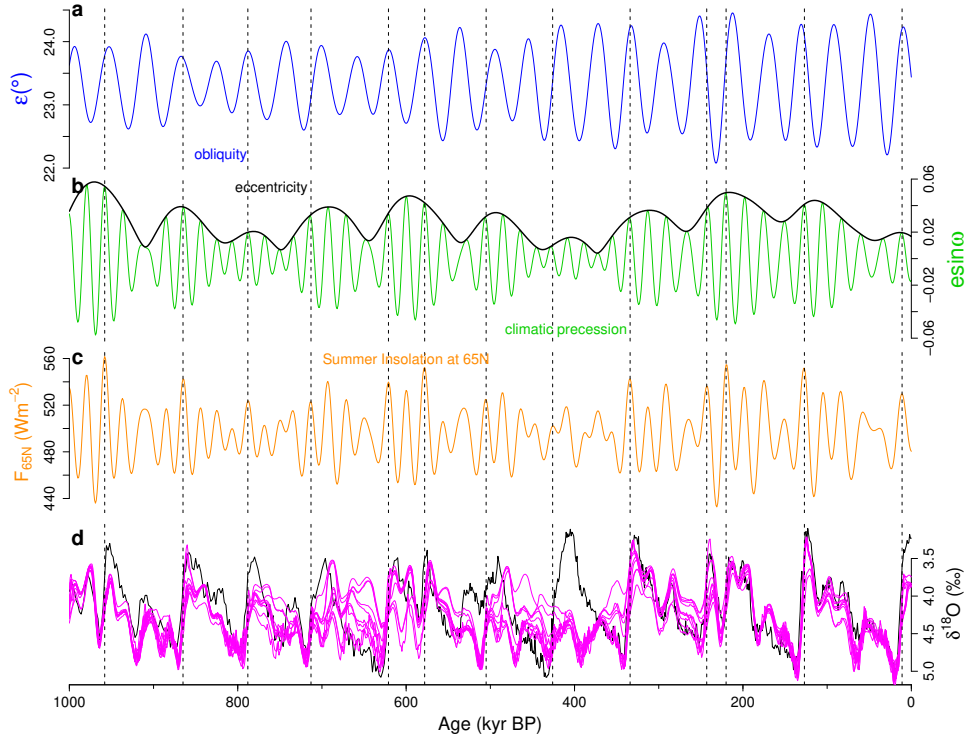
Figure B1. Simulated deglaciations at climatic precession peaks. (a) Obliquity (blue). (b) Climatic precession (green) and eccentricity (black). (c) Boreal summer solstice insolation at $65°$N. (d) LR04 δ^{18}O stack (Lisiecki and Raymo, 2005) (black) representing glacial-interglacial cycles during the last 1 Myr and corresponding CLIMBER-2 δ^{18}O simulations (magenta) under the present background condition regarding the volcanic outgassing rate and the regolith cover. Ten simulations starting from slightly different initial conditions are shown. Note that the vertical axis is reversed so that larger δ^{18}O values, corresponding to colder conditions, are displayed on the lower side. The major deglaciations occur near peaks of climatic precession (i.e., boreal summer insolation peaks) indicated by dashed line, in rising or high phases of eccentricity. The astronomical parameters are from Laskar et al. (2004).

$N = 2^{14}$ in order to increase the number of frequency bins in the periodogram. The periodogram $S(f_k)$ is given for discrete

365 frequencies $f_k = k/(N\Delta t)$ ($k = 1, 2, ..., N/2$, $\Delta t = 1$ kyr). Figure S13 shows the PSDs $S(f)$ calculated for purely periodic series $\sin(2\pi t/T)$ ($t = -1000, ..., -1, 0$ kyr) for periods $T = 405, 124, 95, 82$ and 41 kyr, respectively. Each PSD has the peak near the true frequency $1/T$ but disperses around it because the time length of the analyzed data is not an integer multiple of the signal period; this is commonly referred to as spectral leakage (Bloomfield, 2004). The power of each periodic signal is roughly estimated by integrating the PSD $S(f)$ around the peak frequency $1/T$, i.e., $P_T = \int_{1/T-\Delta f}^{1/T+\Delta f} S(f) df$. The width of

370 the integration interval is specified by Δf. When we want to estimate a power of a frequency component of a multi-frequency signal with frequencies $1/405, 1/124, 1/95, 1/82, 1/41, 1/23.7, 1/22.4$ and $1/19$ kyr^{-1}, the largest Δf that avoids the

overlapping of integration intervals is $\Delta f = (1/82 - 1/95)/2 = 8.34 \times 10^{-4}$ kyr^{-1}. For a purely periodic signal, the band power P_T is about 90% of the total power. Likewise the relative strength of band power is given as $P_T^N = \int_{1/T-\Delta f}^{1/T+\Delta f} S^N(f)df$.

References

390 Abe-Ouchi, A., Saito, F., Kawamura, K., Raymo, M. E., Okuno, J., Takahashi, K., and Blatter, H.: Insolation-driven 100,000-year glacial
cycles and hysteresis of ice-sheet volume, Nature, 500, 190–193, 2013.

Ashkenazy, Y. and Tziperman, E.: Are the 41 kyr glacial oscillations a linear response to Milankovitch forcing?, Quaternary Science Reviews,
23, 1879–1890, 2004.

395 Ashwin, P. and Ditlevsen, P.: The middle Pleistocene transition as a generic bifurcation on a slow manifold, Climate dynamics, 45, 2683–
2695, 2015.

Barker, S., Starr, A., van der Lubbe, J., Doughty, A., Knorr, G., Conn, S., Lordsmith, S., Owen, L., Nederbragt, A., Hemming, S., et al.:
Persistent influence of precession on northern ice sheet variability since the early Pleistocene, Science, 376, 961–967, 2022.

Benzi, R., Parisi, G., Sutera, A., and Vulpiani, A.: Stochastic resonance in climatic change, Tellus, 34, 10–16, 1982.

400 Bereiter, B., Eggleston, S., Schmitt, J., Nehrbass-Ahles, C., Stocker, T. F., Fischer, H., Kipfstuhl, S., and Chappellaz, J.: Revision of the
EPICA Dome C CO2 record from 800 to 600 kyr before present, Geophysical Research Letters, 42, 542–549, 2015.

Berends, C. J., Köhler, P., Lourens, L. J., and van de Wal, R. S. W.: On the Cause of the Mid-Pleistocene Transition, Reviews of Geophysics,
59, e2020RG000 727, https://doi.org/https://doi.org/10.1029/2020RG000727, e2020RG000727 2020RG000727, 2021.

Berger, A., Li, X., and Loutre, M.-F.: Modelling northern hemisphere ice volume over the last 3 Ma, Quaternary Science Reviews, 18, 1–11,
405 1999.

Berger, A., Mélice, J., and Loutre, M.-F.: On the origin of the 100-kyr cycles in the astronomical forcing, Paleoceanography, 20, 2005.

Bintanja, R. and Van de Wal, R.: North American ice-sheet dynamics and the onset of 100,000-year glacial cycles, Nature, 454, 869, 2008.

Bloomfield, P.: Fourier analysis of time series: an introduction, John Wiley & Sons, 2004.

Bosio, A., Salizzoni, P., and Camporeale, C.: Coherence resonance in paleoclimatic modeling, Climate Dynamics, pp. 1–14, 2022.

410 Brovkin, V., Ganopolski, A., Archer, D., and Munhoven, G.: Glacial CO 2 cycle as a succession of key physical and biogeochemical pro-
cesses, Climate of the Past, 8, 251–264, 2012.

Chalk, T. B., Hain, M. P., Foster, G. L., Rohling, E. J., Sexton, P. F., Badger, M. P., Cherry, S. G., Hasenfratz, A. P., Haug, G. H., Jaccard,
S. L., et al.: Causes of ice age intensification across the Mid-Pleistocene Transition, Proceedings of the National Academy of Sciences,
114, 13 114–13 119, 2017.

415 Cheng, H., Edwards, R. L., Sinha, A., Spötl, C., Yi, L., Chen, S., Kelly, M., Kathayat, G., Wang, X., Li, X., et al.: The Asian monsoon over
the past 640,000 years and ice age terminations, nature, 534, 640–646, 2016.

Clark, P. U. and Pollard, D.: Origin of the middle Pleistocene transition by ice sheet erosion of regolith, Paleoceanography, 13, 1–9, 1998.

Clark, P. U., Shakun, J., Rosenthal, Y., Köhler, P., Schrag, D., Pollard, D., Liu, Z., and Bartlein, P.: Requiem for the Regolith Hypothesis:
Sea-Level and Temperature Reconstructions Provide a New Template for the Middle Pleistocene Transition, in: EGU General Assembly
420 Conference Abstracts, pp. EGU21–13 981, 2021.

Crucifix, M.: Oscillators and relaxation phenomena in Pleistocene climate theory, Phil. Trans. R. Soc. A, 370, 1140–1165, 2012.

Crucifix, M.: Why could ice ages be unpredictable?, Climate of the Past, 9, 2253–2267, 2013.

Daruka, I. and Ditlevsen, P. D.: A conceptual model for glacial cycles and the middle Pleistocene transition, Climate dynamics, 46, 29–40,
2016.

425 De Saedeleer, B., Crucifix, M., and Wieczorek, S.: Is the astronomical forcing a reliable and unique pacemaker for climate? A conceptual
model study, Climate Dynamics, 40, 273–294, 2013.

Earth System
Dynamics

Discussions

Open Access

Ditlevsen, P. D.: Extension of stochastic resonance in the dynamics of ice ages, Chemical Physics, 375, 403–409, 2010.

Ford, H. L. and Chalk, T. B.: The Mid-Pleistocene Enigma, Oceanography, 33, 101–103, 2020.

Ganopolski, A. and Brovkin, V.: Simulation of climate, ice sheets and CO 2 evolution during the last four glacial cycles with an Earth system
430   model of intermediate complexity, Climate of the Past, 13, 1695–1716, 2017.

Ganopolski, A. and Calov, R.: The role of orbital forcing, carbon dioxide and regolith in 100 kyr glacial cycles, Climate of the Past, 7,
1415–1425, 2011.

Ganopolski, A., Petoukhov, V., Rahmstorf, S., Brovkin, V., Claussen, M., Eliseev, A., and Kubatzki, C.: CLIMBER-2: a climate system
model of intermediate complexity. Part II: model sensitivity, Climate Dynamics, 17, 735–751, 2001.

435   Ganopolski, A., Calov, R., and Claussen, M.: Simulation of the last glacial cycle with a coupled climate ice-sheet model of intermediate
complexity, Climate of the Past, 6, 229–244, 2010.

Gildor, H. and Tziperman, E.: Sea ice as the glacial cycles' climate switch: Role of seasonal and orbital forcing, Paleoceanography, 15,
605–615, 2000.

Greve, R.: Application of a polythermal three-dimensional ice sheet model to the Greenland ice sheet: response to steady-state and transient
440   climate scenarios, Journal of Climate, 10, 901–918, 1997.

Hagelberg, T., Pisias, N., and Elgar, S.: Linear and nonlinear couplings between orbital forcing and the marine $\delta 18O$ record during the Late
Neocene, Paleoceanography, 6, 729–746, 1991.

Hays, J. D., Imbrie, J., and Shackleton, N. J.: Variations in the Earth's Orbit: Pacemaker of the Ice Ages, Science, 194, 1121–1132, 1976.

Huybers, P.: Combined obliquity and precession pacing of late Pleistocene deglaciations, Nature, 480, 229–232, 2011.

445   Huybers, P. and Wunsch, C.: Obliquity pacing of the late Pleistocene glacial terminations, Nature, 434, 491–494, 2005.

Imbrie, J. and Imbrie, J. Z.: Modeling the climatic response to orbital variations, Science, 207, 943–953, 1980.

Imbrie, J., Boyle, E., Clemens, S., Duffy, A., Howard, W., Kukla, G., Kutzbach, J., Martinson, D., McIntyre, A., Mix, A., et al.: On the
structure and origin of major glaciation cycles 1. Linear responses to Milankovitch forcing, Paleoceanography, 7, 701–738, 1992.

Imbrie, J., Berger, A., Boyle, E., Clemens, S., Duffy, A., Howard, W., Kukla, G., Kutzbach, J., Martinson, D., McIntyre, A., et al.: On the
450   structure and origin of major glaciation cycles 2. The 100,000-year cycle, Paleoceanography, 8, 699–735, 1993.

Imbrie, J. Z., Imbrie-Moore, A., and Lisiecki, L. E.: A phase-space model for Pleistocene ice volume, Earth and Planetary Science Letters,
307, 94–102, 2011.

Jouzel, J., Masson-Delmotte, V., Cattani, O., Dreyfus, G., Falourd, S., Hoffmann, G., Minster, B., Nouet, J., Barnola, J.-M., Chappellaz, J.,
et al.: Orbital and millennial Antarctic climate variability over the past 800,000 years, science, 317, 793–796, 2007.

455   Landa, P. and McClintock, P. V.: Vibrational resonance, Journal of Physics A: Mathematical and general, 33, L433, 2000.

Laskar, J., Robutel, P., Joutel, F., Gastineau, M., Correia, A., and Levrard, B.: A long-term numerical solution for the insolation quantities of
the Earth, Astronomy & Astrophysics, 428, 261–285, 2004.

Le Treut, H. and Ghil, M.: Orbital forcing, climatic interactions, and glaciation cycles, Journal of Geophysical Research: Oceans, 88, 5167–
5190, 1983.

460   Legrain, E., Parrenin, F., and Capron, E.: A gradual change is more likely to have caused the Mid-Pleistocene Transition than an abrupt event,
Communications Earth & Environment, 4, 90, 2023.

Liautaud, P. R., Hodell, D. A., and Huybers, P. J.: Detection of significant climatic precession variability in early Pleistocene glacial cycles,
Earth and Planetary Science Letters, 536, 116 137, 2020.

Lisiecki, L. E.: Links between eccentricity forcing and the 100,000-year glacial cycle, Nature geoscience, 3, 349–352, 2010.

Earth System
Dynamics

Discussions

465   Lisiecki, L. E. and Raymo, M. E.: A Pliocene-Pleistocene stack of 57 globally distributed benthic δ18O records, Paleoceanography, 20, 2005.

Lüthi, D., Le Floch, M., Bereiter, B., Blunier, T., Barnola, J.-M., Siegenthaler, U., Raynaud, D., Jouzel, J., Fischer, H., Kawamura, K., et al.: High-resolution carbon dioxide concentration record 650,000–800,000 years before present, Nature, 453, 379–382, 2008.

Maasch, K. A. and Saltzman, B.: A low-order dynamical model of global climatic variability over the full Pleistocene, Journal of Geophysical Research: Atmospheres, 95, 1955–1963, 1990.

470   Matteucci, G.: Orbital forcing in a stochastic resonance model of the Late-Pleistocene climatic variations, Climate Dynamics, 3, 179–190, 1989.

Milankovitch, M.: Kanon der erdbestahlung und seine anwendung auf das eiszeitproblem, 133, Königlich Serbische Academie, Belgrade, 1941.

Mitsui, T. and Aihara, K.: Dynamics between order and chaos in conceptual models of glacial cycles, Climate dynamics, 42, 3087–3099, 475   2014.

Mitsui, T. and Crucifix, M.: Effects of additive noise on the stability of glacial cycles, Mathematical Paradigms of Climate Science, pp. 93–113, 2016.

Mitsui, T., Crucifix, M., and Aihara, K.: Bifurcations and strange nonchaotic attractors in a phase oscillator model of glacial–interglacial cycles, Physica D: Nonlinear Phenomena, 306, 25–33, 2015.

480   Mori, T. and Kai, S.: Noise-induced entrainment and stochastic resonance in human brain waves, Physical review letters, 88, 218 101, 2002.

Nicolis, C.: Solar variability and stochastic effects on climate, Solar Physics, 74, 473–478, 1981.

Nyman, K. H. and Ditlevsen, P. D.: The middle Pleistocene transition by frequency locking and slow ramping of internal period, Climate Dynamics, 53, 3023–3038, 2019.

Paillard, D.: The timing of Pleistocene glaciations from a simple multiple-state climate model, Nature, 391, 378–381, 1998.

485   Paillard, D.: Glacial cycles: toward a new paradigm, Reviews of Geophysics, 39, 325–346, 2001.

Parrenin, F. and Paillard, D.: Terminations VI and VIII (∼530 and ∼720 kyr BP) tell us the importance of obliquity and precession in the triggering of deglaciations, Climate of the Past, 8, 2031–2037, 2012.

Pelletier, J. D.: Coherence resonance and ice ages, Journal of Geophysical Research: Atmospheres, 108, 2003.

Petit, J.-R., Jouzel, J., Raynaud, D., Barkov, N. I., Barnola, J.-M., Basile, I., Bender, M., Chappellaz, J., Davis, M., Delaygue, G., et al.:
490   Climate and atmospheric history of the past 420,000 years from the Vostok ice core, Antarctica, Nature, 399, 429–436, 1999.

Petoukhov, V., Ganopolski, A., Brovkin, V., Claussen, M., Eliseev, A., Kubatzki, C., and Rahmstorf, S.: CLIMBER-2: a climate system model of intermediate complexity. Part I: model description and performance for present climate, Climate dynamics, 16, 1–17, 2000.

Pikovsky, A., Kurths, J., Rosenblum, M., and Kurths, J.: Synchronization: a universal concept in nonlinear sciences, 12, Cambridge university press, 2003.

495   R Core Team: R: A Language and Environment for Statistical Computing, R Foundation for Statistical Computing, Vienna, Austria, https://www.R-project.org/, 2020.

Raymo, M.: The timing of major climate terminations, Paleoceanography, 12, 577–585, 1997.

Raymo, M. E., Lisiecki, L., and Nisancioglu, K. H.: Plio-Pleistocene ice volume, Antarctic climate, and the global δ18O record, Science, 313, 492–495, 2006.

500   Rial, J. A.: Pacemaking the ice ages by frequency modulation of Earth's orbital eccentricity, Science, 285, 564–568, 1999.

Rial, J. A.: Abrupt climate change: chaos and order at orbital and millennial scales, Global and planetary change, 41, 95–109, 2004.

Earth System
Dynamics

Discussions

Ridgwell, A. J., Watson, A. J., and Raymo, M. E.: Is the spectral signature of the 100 kyr glacial cycle consistent with a Milankovitch origin?, Paleoceanography, 14, 437–440, 1999.

Riechers, K., Mitsui, T., Boers, N., and Ghil, M.: Orbital insolation variations, intrinsic climate variability, and Quaternary glaciations, Climate of the Past, 18, 863–893, 2022.

Rohling, E., Foster, G. L., Grant, K., Marino, G., Roberts, A., Tamisiea, M. E., and Williams, F.: Sea-level and deep-sea-temperature variability over the past 5.3 million years, Nature, 508, 477–482, 2014.

Saltzman, B., Maasch, K., and Hansen, A.: The late Quaternary glaciations as the response of a three-component feedback system to Earth-orbital forcing, Journal of the Atmospheric Sciences, 41, 3380–3389, 1984.

Snyder, C. W.: Evolution of global temperature over the past two million years, Nature, 538, 226–228, 2016.

Spratt, R. M. and Lisiecki, L. E.: A Late Pleistocene sea level stack, Climate of the Past, 12, 1079–1092, 2016.

Strogatz, S. H.: Nonlinear dynamics and chaos: with applications to physics, biology, chemistry, and engineering, CRC Press, 2018.

Tzedakis, P., Crucifix, M., Mitsui, T., and Wolff, E. W.: A simple rule to determine which insolation cycles lead to interglacials, Nature, 542, 427–432, 2017.

Verbitsky, M. Y., Crucifix, M., and Volobuev, D. M.: A theory of Pleistocene glacial rhythmicity, Earth System Dynamics, 9, 1025–1043, 2018.

Watanabe, Y., Abe-Ouchi, A., Saito, F., Kino, K., O'ishi, R., Ito, T., Kawamura, K., and Chan, W.-L.: Astronomical forcing shaped the timing of early Pleistocene glacial cycles, Communications Earth & Environment, 4, 2023.

Willeit, M., Ganopolski, A., Calov, R., and Brovkin, V.: Mid-Pleistocene transition in glacial cycles explained by declining CO2 and regolith removal, Science Advances, 5, eaav7337, 2019.

Willeit, M., Ganopolski, A., Robinson, A., and Edwards, N. R.: The Earth system model CLIMBER-X v1. 0–Part 1: Climate model description and validation, Geoscientific Model Development, 15, 5905–5948, 2022.

Willeit, M., Ilyina, T., Liu, B., Heinze, C., Perrette, M., Heinemann, M., Dalmonech, D., Brovkin, V., Munhoven, G., Börker, J., et al.: The Earth system model CLIMBER-X v1. 0–Part 2: The global carbon cycle, Geoscientific Model Development Discussions, pp. 1–47, 2023.

Zhou, C., Kurths, J., Allaria, E., Boccaletti, S., Meucci, R., and Arecchi, F.: Noise-enhanced synchronization of homoclinic chaos in a CO 2 laser, Physical Review E, 67, 015 205, 2003.